



Evaluation of Protective Cavities Position on Decreasing Destructive Effects of Surface Blast on Buried Tunnels

H. Hosseini-Nassab¹, S.M. Movahedifar^{2,*}

¹M.Sc. of Civil Eng., Young Researchers and Elites Club, Birjand branch, Islamic Azad University, Birjand, Iran.

²Assistant Professor, Department of civil, Neyshabur Branch, Islamic Azad University, Neyshabur, Iran.

ABSTRACT: In recent years, in the wake of growing military and terrorist threats especially against strategic and social buried structures, immunization of these structures against explosions becomes a major necessity. Therefore, it is crucial to study and use efficient methods to provide practical solutions to protect the key structures against advanced weapons and bombs. In this paper, the phenomenon of surface explosion and its impact on the tunnels, which are the most important buried structures, has been studied in full detail in a 3D environment. Additionally, evaluated the effect of depth, number, and location of the tunnel protective cavities in reducing destructive effects of the explosions on the tunnels in a 2D environment using nonlinear dynamic analysis in ANSYS-AUTODYN software. The results indicate that increasing the depth and number of the tunnel protective cavities are effective in reducing the destructive effects of the explosion on buried tunnels. As a key finding, the best location of the tunnel cavities was estimated in the range between the edges of the tunnel section and the edges of explosion charge.

Review History:

Received: Sep. 24, 2019

Revised: Jan. 07, 2020

Accepted: Jan. 11, 2020

Available Online: Feb. 04, 2020

Keywords:

Buried Tunnel

Surface Explosion

Immunization

AUTODYN

1- Introduction

comparison to typical static and phenomenon is much more complicated. This is mainly due to its highly dynamic nature and lack of related empirical studies. Here, the complexity of the soil environment and burial depth of the tunnels has added to the difficulties and therefore laboratory experiments on the interaction of tunnels and explosive phenomena are very costly and technically challenging. As a cost-efficient and promising approach, finite element modeling of the impact of surface explosions on the buried structure has become more popular. In particular, references [1] and [2] compared the behavior of 2D and 3D models of the buried structures during the explosion. They analyzed the dynamic response of the structures to the facing explosion waves using a smoothed particle hydrodynamics (SPH) model for simulating high-deformation zones in the geometry and a Lagrangian model for the other parts. They concluded that the 2D model had acceptable results for explosive analyzes. In another study, it modeled an explosion condition in the ANSYS-AUTODYN hydrocode [3]. They focused on the shape of charge and crater in large-scale explosions and concluded that the dimensions of the crater formed in the underlying soil depend on the explosive layout. Explosion crater parameters were the subject of researchers in reference [4]. They modeled a rectangular tunnel in the ground and an explosion with 100 kilograms of TNT on the ground surface to investigate the behavior of the tunnel roof and crater parameters. They also evaluated the failure of the

*Corresponding author's email: Movahedi_far@yahoo.ca

tunnel structure using ABAQUS/explicit software. Reference [5] studied the dynamic response of underground arched structures to the explosive waves and compared two models for fluid-structure interaction concerning the time history of acceleration, speed, and displacement calculated on different locations of the model. They recommended constructing the buried structures in soil with lower sound speed and a larger reduction factor to reduce the drawbacks of a possible explosion. In reference [6] it examined the effects of the bolts on the robustness of the tunnel movement caused by the explosion waves. They used AUTODYN software and confirmed the significant effects of bolts in the prevention of severe displacement of the tunnels due to explosions. Finally, reference [7] evaluated the displacement and pressure at three different points in tunnel structure with Cobe box-shaped sections using LS-DYNA hydrocode and concluded that the largest displacement occurs on the tunnel roof, exactly below the explosion charge (which was slightly larger than that of the corner of the roof).

As you can read in these studies, it seemed that there were many studies about the types of explosions and their effect on buried structures, but there were not enough studies on the effect of empty spaces in protecting the tunnel against surface blasts, so we tried to evaluate the effectiveness of tunnel immunization using protective cavities. We used 2D along with 3D models to save the analysis time. Autodyn integrated hydrocode was utilized due to its excellent graphics environment, ease of use, and integration in preprocessing and post-processing environments.



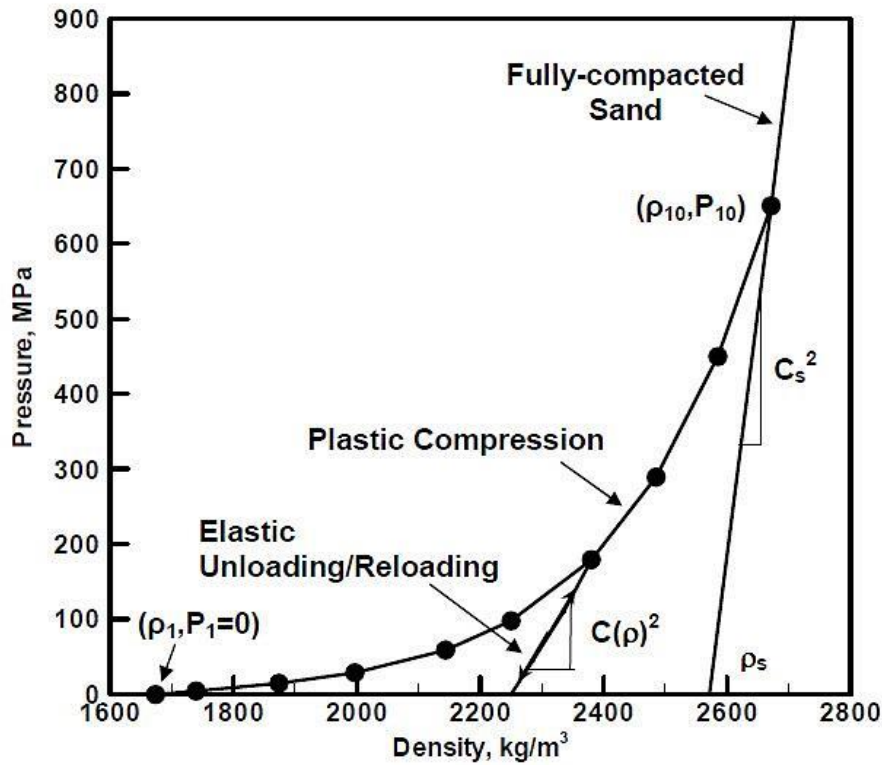


Fig. 1. Ten part density- pressure diagram of the soil [8]

2- Materials and methods

2.1. Soil

Compaction equation of state (EOS) for soil presented in reference [8] was used in this study. The compaction EOS is obtained from a three-axial test to define soil states at different pressures using a pressure-density curve (Fig.1.).

The compaction EOS defining porous materials such as soil is a special form of Mie-Gruneisen EOS in which the second term is omitted.

$$P = P_H + \Gamma_\rho (e - e_H) \quad (1)$$

Where P (Pa) is the total pore and effective pressure in the soil skeleton, ρ (kg/m^3) is current soil density, Γ (N.m/J) is gamma Gruneisen parameter and e (J/kg) is the internal energy density. The subscript H denotes the Hugoniot shock level reference that is a countable quantity obtained from an equation that shows the shock process using thermodynamic law. It is assumed that pressure in the soil does not depend on internal energy and therefore the equation is equivalent to the standard Mie-Gruneisen EOS in which the gamma parameter is considered to be zero. This model also gives more reliable answers when the absorbed energy is not high, the initial porosity of the material is low or the gamma parameter is close to zero [9].

Other values of the variables based on soil type 5 are available in the reference [10].

2.2. TNT

We used Jones-Wilkins-Lee (JWL) equation to define the TNT charge to the software. JWL is a fundamentally physical model that simulates chemical explosives using thermodynamic laws [11].

$$P = A \left(1 - \frac{W}{VR_1}\right) e^{-VR_1} + B \left(1 - \frac{W}{VR_2}\right) e^{-VR_2} + \frac{W}{V} E \quad (2)$$

Where A , B , $R1$, $R2$, and W are constants that are specific to the explosive and can be extracted through experimental tests. E is the energy per unit volume in mega-bar and V is the volume of the products from the explosion process to the initial volume of the explosive or their density [12]. Related specifications for TNT standard explosives with a density of $1.63 \text{ g}/\text{cm}^3$ are listed in Table 1.

2.3. Air

For the air environment, we used the following equation that is appropriate for defining ideal gases [13].

$$G = C_p / C_v \quad (3)$$

Table 1. The most important specifications of TNT

TNT		
Equation of State	JWL	
Reference density	1/63	g/cm ³
Parameter A	373770000	kPa
Parameter B	3747100	kPa
Parameter R1	4/15	---
Parameter R2	0/9	---
Parameter W	0/35	---

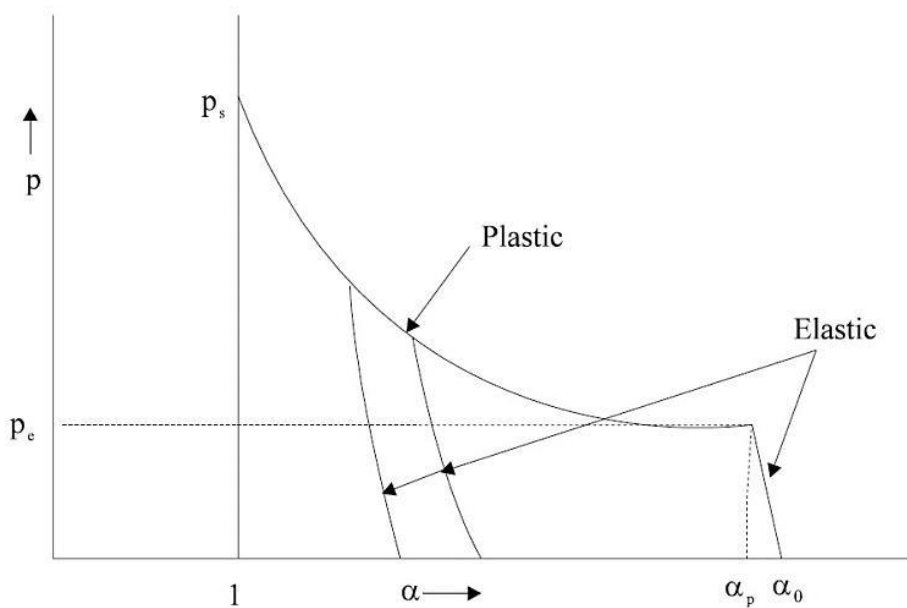


Fig. 2. Relationship between the pressure and porosity of materials (P- α equation) [20].

Where ρ (kg/m³) is density, P (Pa) denotes the pressure and G is the ratio of the specific heat coefficients in the condition of constant pressure to that obtained in the constant volume condition:

$$G = C_p / C_v \quad (4)$$

G is equal to 1.4 at low pressures but because of decomposition and ionization at high pressures and temperatures, its value does not exceed 1.4 [14]. At the gas temperature T (°K), the initial internal energy e (kJ/kg), is the product of the specific heat in the constant volume C_v [15]. In the Autodyn library, the initial air density was set to 225/1 (kg/m³), the reference temperature was 288.2 (°K), the special temperature in the constant volume was 717.66 (J/kg.°K), the special temperature at the constant pressure was 1004.64 (J/kg.°K). and the value of e was 206812 (kJ/kg)

[16]. Moreover, it was not necessary to define the strength and failure relationships for gases because they have no resistance to shear stresses or negative pressures [9].

2.4. Concrete

Concrete can be assumed isotropic before the moment of failure if the concrete is well mixed and vibrated [17]. Concrete behavior under dynamic and shock loads is a complex nonlinear phenomenon, which is completely different from its behavior under static loads [18]. Therefore, in this paper, we used the RHT (Reidel-Hiermaier-Thoma) model to describe brittle materials such as concrete under dynamic loads [19]. The RHT model is presented as yielding stress curves in which the pressure is defined as the average of the three main stresses [20]. For the current study, the RHT model was used to model the resistance and failure behavior of concrete and the P- α model was used as EOS. Fig. 2. shows the relationship between the pressure and porosity of the materials that are known as the P- α equation.

Table 2. Major characteristics of concrete

CONCRETE		
Equation of State		P alpha
Reference density	2/75	g/cm ³
Porous density	2/314	g/cm ³
Porous sound speed	2920	m/s
Initial compaction pressure	23300	kPa
Solid compaction pressure	6000000	kPa
Bulk Modulus	35270000	kPa
Failure		RHT Concrete
Minimum Strain to Failure	0/01	---
Strength		RHT Concrete
Shear Modulus	16700000	kPa
Compressive Strength (fc)	35000	kPa
Tensile Strength (ft/fc)	0/01	---
Shear Strength (fs/fc)	0/18	---

Table 3. The most important characteristics of steel

STEEL		
Equation of State	Shock	
Reference density	7/896	g/cm ³
Reference Temperature	300	°K
Specific Heat	452	J/kg°K
Strength	Johnson Cook	
Shear Modulus	81800000	kPa
Yield Stress	350000	kPa
Hardening Constant	275000	kPa
Hardening Exponent	0/36	---
Strain Rate Constant	0/022	---
Melting Temperature	1811	°K

In this diagram, α represents the porosity of the materials and is expressed by:

$$\alpha = V/V_s \quad (5)$$

Where V is the volume of the porous material and V_s is the volume of the solid part of the material (without empty spaces). The advantage of the P- α model in comparison with other models is that this model is suitable for representing the behavior of the brittle-porous materials in high and low stresses. Therefore, a range of stresses and properties are defined using only a single formula. In full compression conditions, $\alpha = 1$ [20] and other specifications for concrete

are given in Table2.

Steel

Steel was used to model the reinforcing elements in the concrete structure. There is a linear EOS describing the linear behavior between volumetric strain and pressure in the steel that is linked to each other by the bulk modulus (K). In the current study, the Johnson-Cook model was used to define the mechanical behavior of steel. The Johnson-Cook model is using the hardness effects, strain rate, and temperature to simulate the steel behavior under shock and explosion conditions. In addition, a failure model based on the plastic strain was used to estimate the failure [21]. Some of the most important specifications of steel are reported in Table3.

Table 4. Important specifications used for modeling of blast wave propagation

Parameter	Amount	Unit
Distance to the Explosion (R)	1-18	m
Coupling Factor (f)	0.4	---
Acoustic Impedance ($\rho_c \times 10^5$)	4.977	Pa.s/m
Charge Weight (W)	205	kg
Attenuation Coefficient (n)	2.75	---

3- Blastwave propagation in the soil

In the explosion phenomenon, after the activation of detonation, explosive charges cause a rapid increase in temperature and pressure and produce dense and massive gases. The hot and high-pressure gas becomes a powerful source of waves in the environment that can quickly propagate in the soil [22]. The stresses induced to the ground by the explosion are much higher than those caused by explosions in the air, both in terms of severity and loading time [10]. The loading applied by a surface explosion wave was determined by the waveform, maximum overpressure P_{s0} , and duration of the wave t_d . P_{s0} is estimated by the following semi-empirical formula, referred to TM5-855-1 technical manual (USA Fundamentals of protective design for conventional weapons).

$$V_0 = 48.768f \left(\frac{2.52R}{W^{\frac{1}{3}}} \right)^{-n} \quad (6)$$

$$P_{s0} = 22620.59 \rho_c V_0 \quad (7)$$

Where P_{s0} is the peak pressure in the free field in Pascal, R (m) is the distance between the center of the charge and the target in meters, V_0 is the peak particle velocity in m/s and f is the coupling factor (it can be defined based on the information provided by [10] using the scaled distance). In this study, f is 0.4 because the blast takes place on the surface of the soil. ρ_c is the acoustic impedance in Pa.s/m, W is the explosive charge weight in kilograms, n is the attenuation coefficient (soil damping coefficient), which was set to 2.75 in this study ([10] assuming the soil type 5). The main parameters used for modeling blast wave propagation are listed in Table 4.

4. Geometric model – results and discussions

The following assumptions were made for the current study:

- The soil properties were assumed constant at different depths.
- All materials were considered isotropic.
- Static loads were ignored as they are very small in

comparison with explosive loads.

- The groundwater level was assumed to be lower than the tunnel and therefore did not influence the analysis.

Three-dimensional geometry and Eulerian environment were used to investigate the blast wave propagation in the soil. Fig.3 shows the 3D geometry in which explosives, soil, and air were modeled in the Eulerian environment. Eighteen sensors have been placed to record the pressure history in different parts of the soil environment (below the explosive charge in 1-meter intervals).

The 20×20×20 meters soil environment was represented by SAND material with a density of 3641 g/cm³, Compaction EOS, Mo-Granular strength, and Hydro failure model (P min). Air was modeled as an ideal gas using 20x20x5m air materials and the explosive volume was equal to 205 kg of TNT modeled by JWL EOS, with a density of 1630 kilogram per cubic meter. The soil, air, and explosives were modeled in a 3D integrated Euler environment. By integrating the Eulerian environment, Eulerian-Eulerian communication of explosives, air, and soil was identified for the software. The materials flow boundary (Flow Out), was used to introduce boundaries of the air environment with the external surface of the model. Moreover, for taking into account the interaction of soil and exterior face of the model, a Transmit energy (transmission) condition was defined (see Figure 4.). These boundary conditions allow materials to flow and transfer energy and waves without affecting other sectors. An explosive detonator was defined as a point at the top of the explosive charge (as in reality, the greater concentration of explosion wave was assumed to be on the soil environment). Stress distribution in the model captured in an instance during the analysis is depicted in Fig.4

Surface blast wave propagates with a hemisphere shape in the soil and air, but its propagation in the soil is more complicated because the mechanical behavior of the soil environment is more complex than the air.

After completion of the analysis, the graph of the maximum overpressure recorded by the sensors at various depths was compared against the results obtained from Eq. (7) derived from the TM5-855-1. The comparison indicates a very good agreement (86.4%) (See Fig. 5).

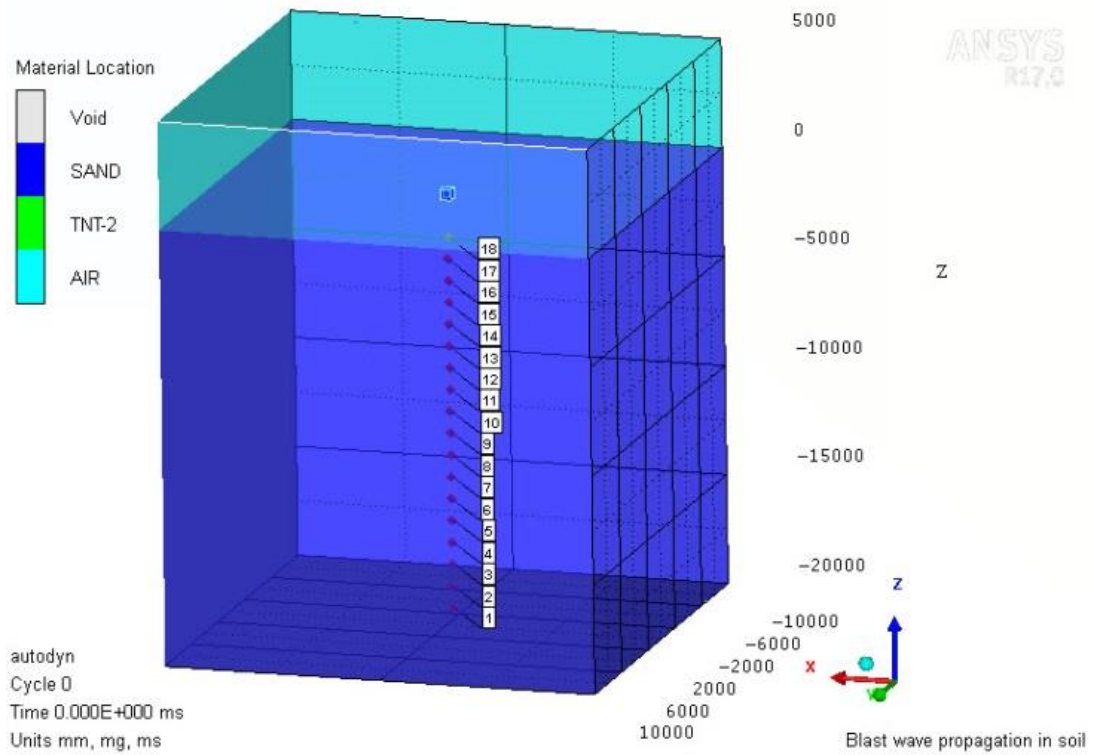


Fig. 3. The geometry of the model for the blast wave propagation in the soil with the positioning of the materials and gages.

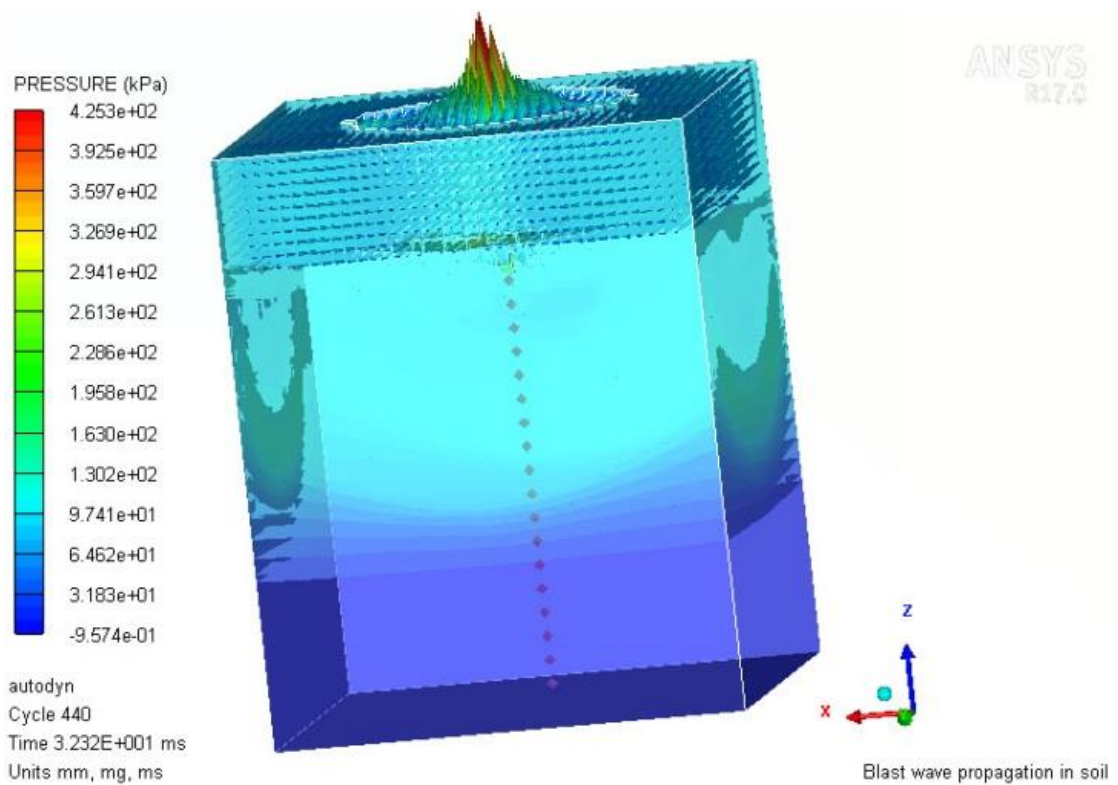


Fig. 4. Stress distribution in the model in a time instance during analysis.

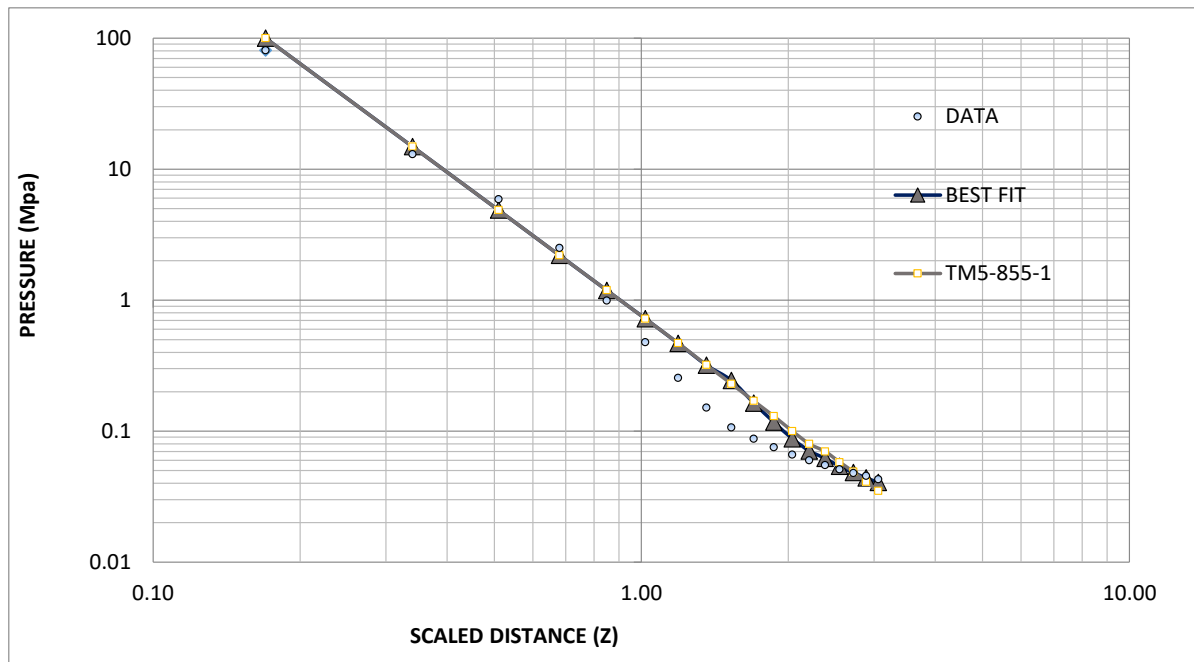


Fig. 5. Comparison of the analysis results with the corresponding values obtained from the formulas provided in the US code TM5-855-1.

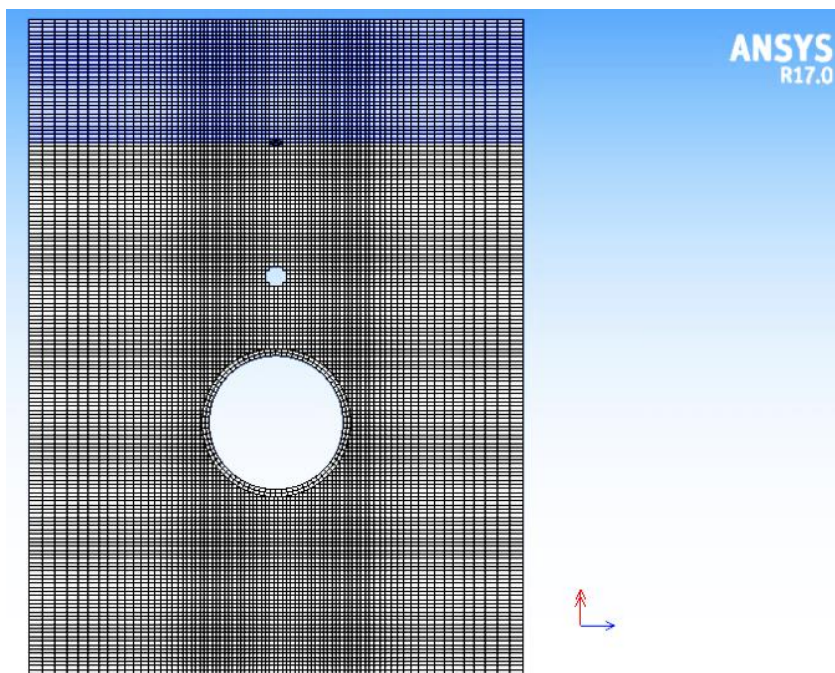


Fig. 6. Model geometry, meshing, and protective cavity.

4.1. Effects of the positioning of the protective cavities on the destructive impacts of the surface blast

A circular tunnel section together with circular protective cavities around the tunnel was modeled and the effectiveness of cavities in reducing impacts of an explosion on the tunnel structure was evaluated. Fig.6 and Fig.7 illustrate the model geometry, meshing, boundaries, soil environment, air,

explosives, and a protective cavity. Our model, its interactions, and boundaries were like we described it before in section 3, only for taking into account the interaction of soil and tunnel we used Euler-Lagrange interaction. It means all parts were introduced to the software in the Eulerian environment and the only tunnel was introduced in a Lagrange environment to hydrocode.

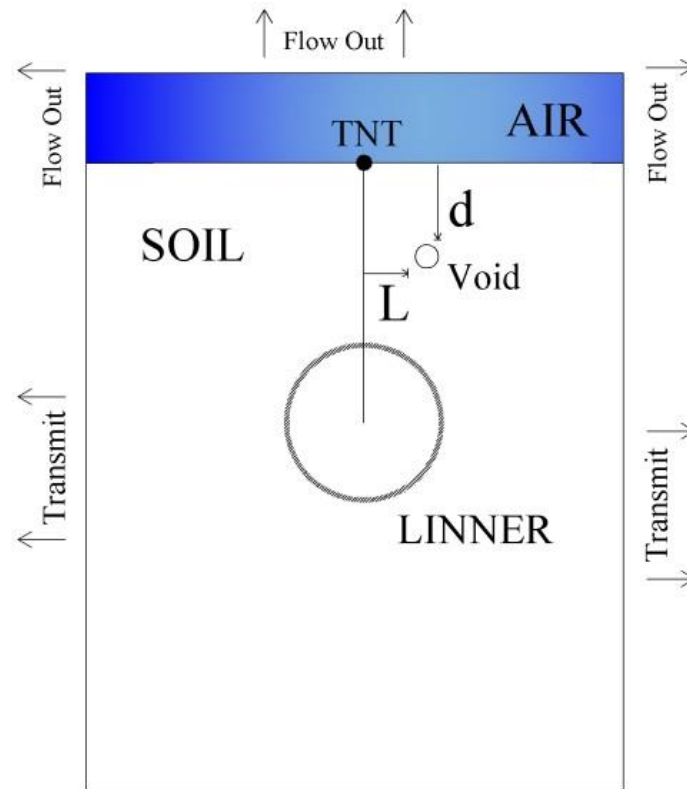


Fig. 7. Schematic model geometry and boundaries.

After the detonator is functioning, the explosive charge activates and explodes. Since the detonator is above the charge, the focus of the waves will be on the ground. The blast waves radiate away from the charge and hit the cavities in the path and then hit the body of the tunnel. Waves will move particles (soil and tunnel) and put pressure on them. Fig.8.

The gridded mesh was used to save the analysis time and achieve acceptable accuracy. Since programs dealing with high strain rates use complex equations and algorithms, they require huge processing power; therefore, the following considerations were taken into account to optimize the analysis performance. An axisymmetric model including a circular tunnel section, two layers of reinforcement with 35 cm thickness (this type of tunnel structure is more common nowadays), and a protective cavity with 1m diameter was used. The model was subjected to 205 kg of TNT explosive charges. Effects of protective cavities in different depths ($d=3.5, 4, 6,$ and 7.5 meters) from the explosive charge, while the other parameters were fixed to their baseline values, were assessed. In the second step, the depth and other parameters were constant, and the only effect of the shift of cavities center from the wave axis ($L=0, 0.5, 1, 1.5, 2,$ and 2.5 meters) was studied. In the third and fourth steps, one cavity was placed in the optimum position obtained from the second step and studied effects of a second cavity in the lower and upper layers of soil relative to the first cavity. Finally, based

on the results obtained in the previous steps, we studied three axial, symmetric crinkle, and asymmetric crinkle modes, to estimate the proper arrangement of the cavities in presence of the third cavity.

In this section, all the parameters were kept constant and the effect of changing the depth of protective cavities was studied. Cavities were placed in different depths (3, 4.5, 6, and 7.5 meters) and the analyses were performed. The distribution of pressure lines in a time instance during analysis is shown in Fig.8.

After completion of the analysis, time-effective strain diagrams at each studied depth (in the most critical point of the tunnel structure) were showed in Fig.9.

Based on these results, if the cavities are excavated closer to the tunnel structure, they can provide a higher safety level by reducing the destructive effects on the tunnel.

4.3. Distance of protective cavities from the wave axis (L)

In the second step, all the parameters, including the depth of the cavity from the soil surface, were kept constant and only perturbed the distance (L) between the cavity from the wave axis (from 0 to 2.5 m with 0.5 m intervals). Results are illustrated in Fig.10.

As we found, the protective effect of the cavity when it was aligned with the axis of the explosion wave, was lower than the cavities in the range of approximately 0.5 to 1.5 times of the cavity diameter from the wave axis. The reason

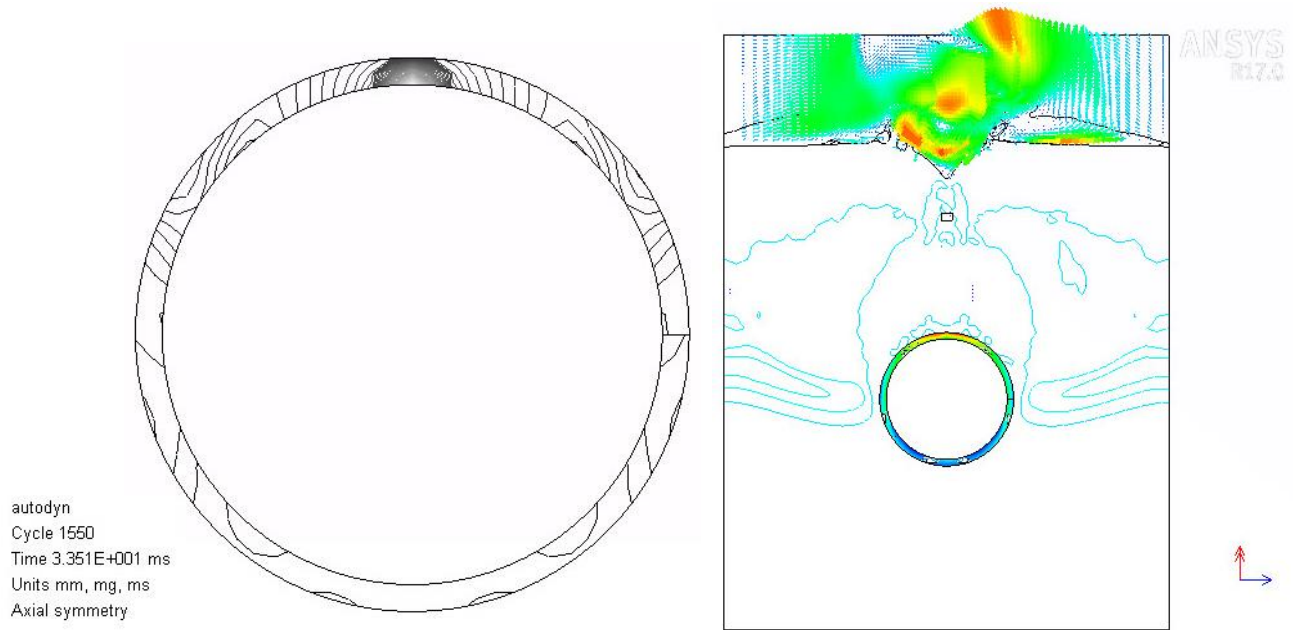


Fig. 8. Distribution of pressure lines in a time instance during analysis.

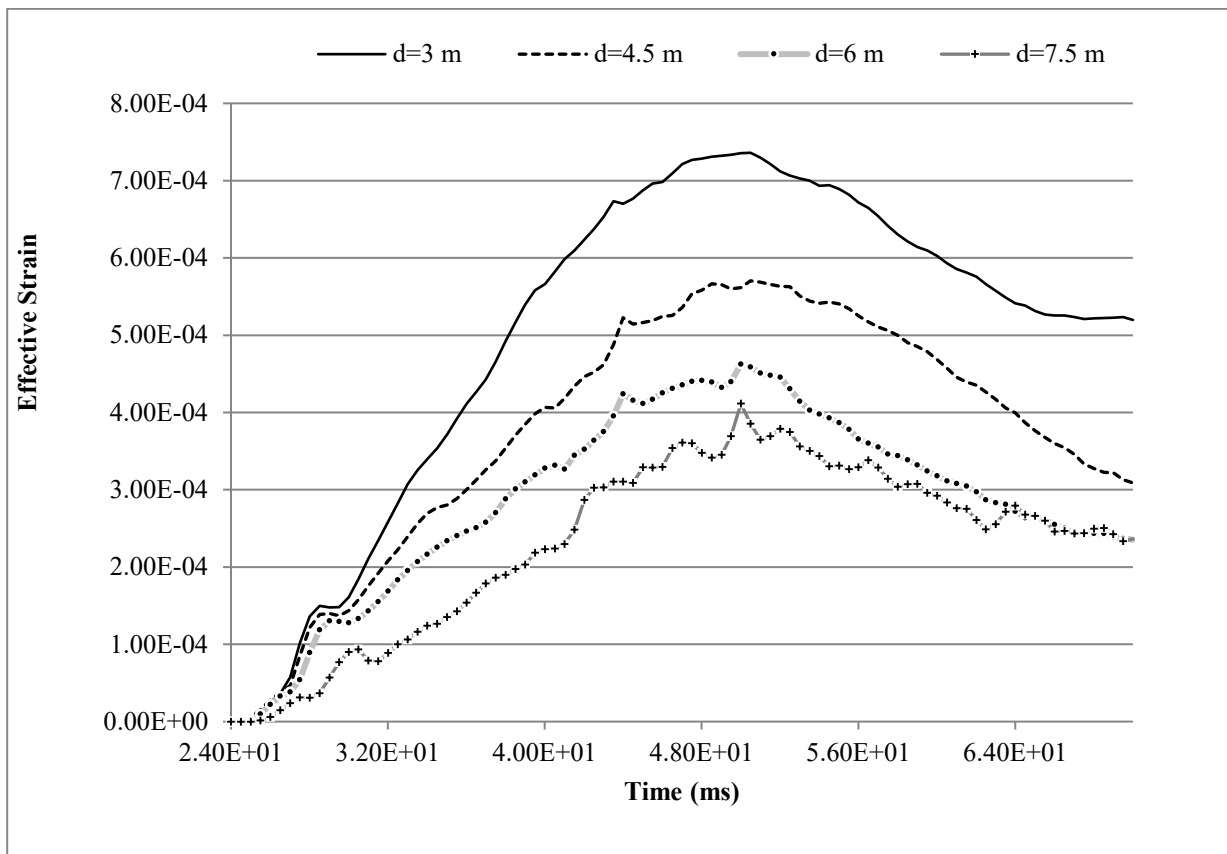


Fig. 9. Effect of changing the depth of cavity (d).

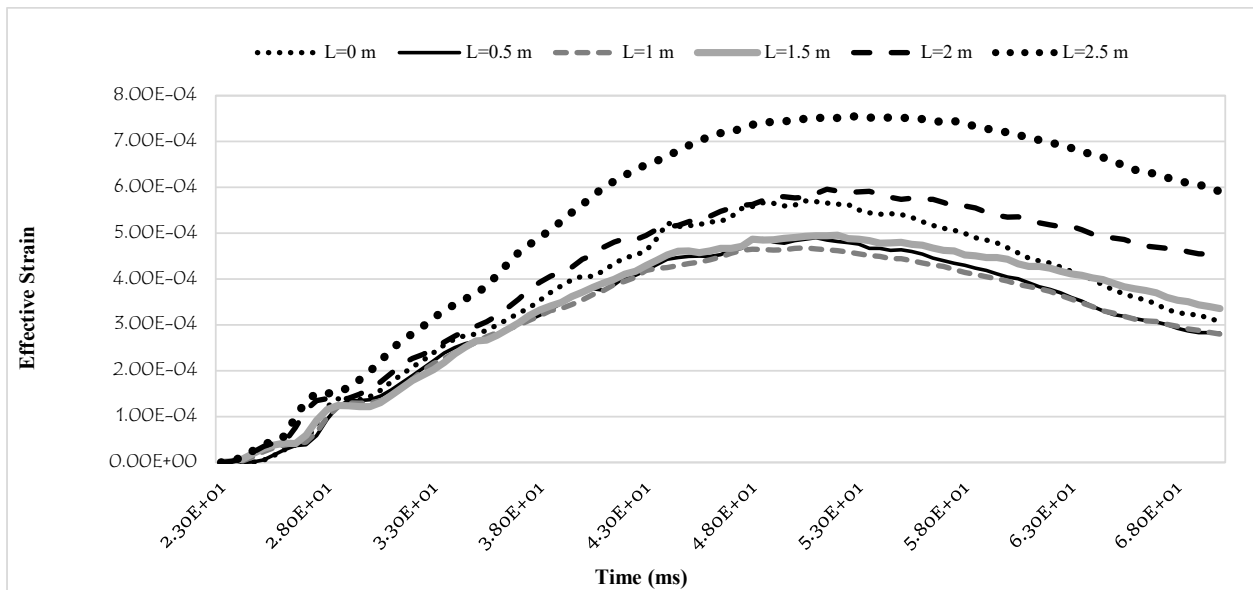


Fig. 10. Results for shifting the cavities from the blast wave axis (L).

might be when the center of the cavity is exactly on the wave axis, disruption and disturbance in the path of the explosive wave are less than when the cavities are in the range of 0.5 to 1.5 times of protective cavity diameter from the wave axis. Moreover, based on the results, cavities outside the range between the edges of the tunnel section and charge edges had no considerable effect on reducing the explosive wave loads. So the optimum range for the protective cavities is between 0.5 and 1.5 times the cavity diameter from the wave axis.

4.4. Effect of the number of cavities around the tunnel and their positions

In another part of the study, the effect of the number of cavities (more than one loop) on reducing the destructive effects of the explosion was investigated. Keeping the first cavity in a fixed position (the optimum position obtained from the results of the previous step), the second cavity was placed one and a half meter apart from the bottom of the first cavity and the role of the distance of the second cavity from the wave axis on the explosion impact was studied Fig.11. Results are depicted in Fig.12.

According to the results plotted in Fig.12. when the second cavity is used, it is recommended to place it in the range of approximately 0.5 to 1.5 times the cavity diameter from the wave axis. Moreover, to obtain a better protective effect, it is recommended to place the first cavity on the opposite side of the wave axis.

The optimum position of the protective cavities when using three loops of the cavities: axial direction, asymmetric crinkle, and symmetric crinkle were studied. In the symmetric case, L (distance between the cavity and the wave axis) for the two loops on both sides of the wave axis was equal (see Fig.13.). The analysis results for this case are reported in Fig.14.

Based on the results depicted in Fig.14. in the case of multi-layer cavities, they should be arranged in a crinkle and preferably asymmetric layout. Finally, results plotted in Fig.15. suggest the positioning of the protective cavities is the range between tunnel and charge edges (shaded area).

A simple example can better explain why cavities should not be along the wave axis. When water flows from an open tap, one can cross the water path by moving his/her finger slowly from the side to the center of the flow. This results in the distraction of the water particles that become more concentrated when the finger reaches the center of the flow. In other words, the area protected against the water pressure becomes smaller and finally, only a small area located under the finger is protected against the water pressure.

5- Conclusions

In this study, the mechanical condition of buried tunnels during surface explosion was simulated using ANSYS-AUTODYN software. 2D and 3D geometry of the tunnel structure, soil, air, and explosive environments were modeled. Effects of some important parameters such as depth of the tunnel protective cavities, their distance from the wave axis, number of cavities around the tunnel, and their position were evaluated. The results indicated higher protection when cavities are placed closer to the tunnel structure. The

optimum range for positioning the protective cavities was found between 0.5 and 1.5 times the cavity diameter from the wave axis and in the range between the edges of the tunnel section and the edges of explosive charge. Increasing the number of protective cavities can result in better protection, provided that they are in the range mentioned above. Finally, our findings recommended the arrangement of multi-layer cavities in asymmetric crinkle layouts.

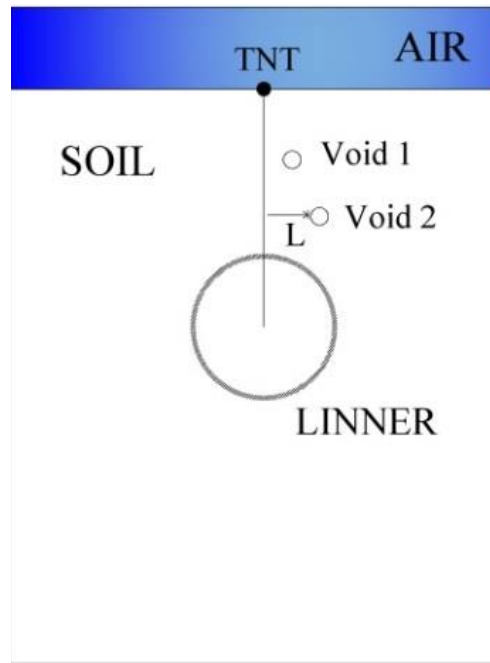


Fig. 11. Schematic of the model geometry used for assessing the effect of the number of cavities around the tunnel and their position.

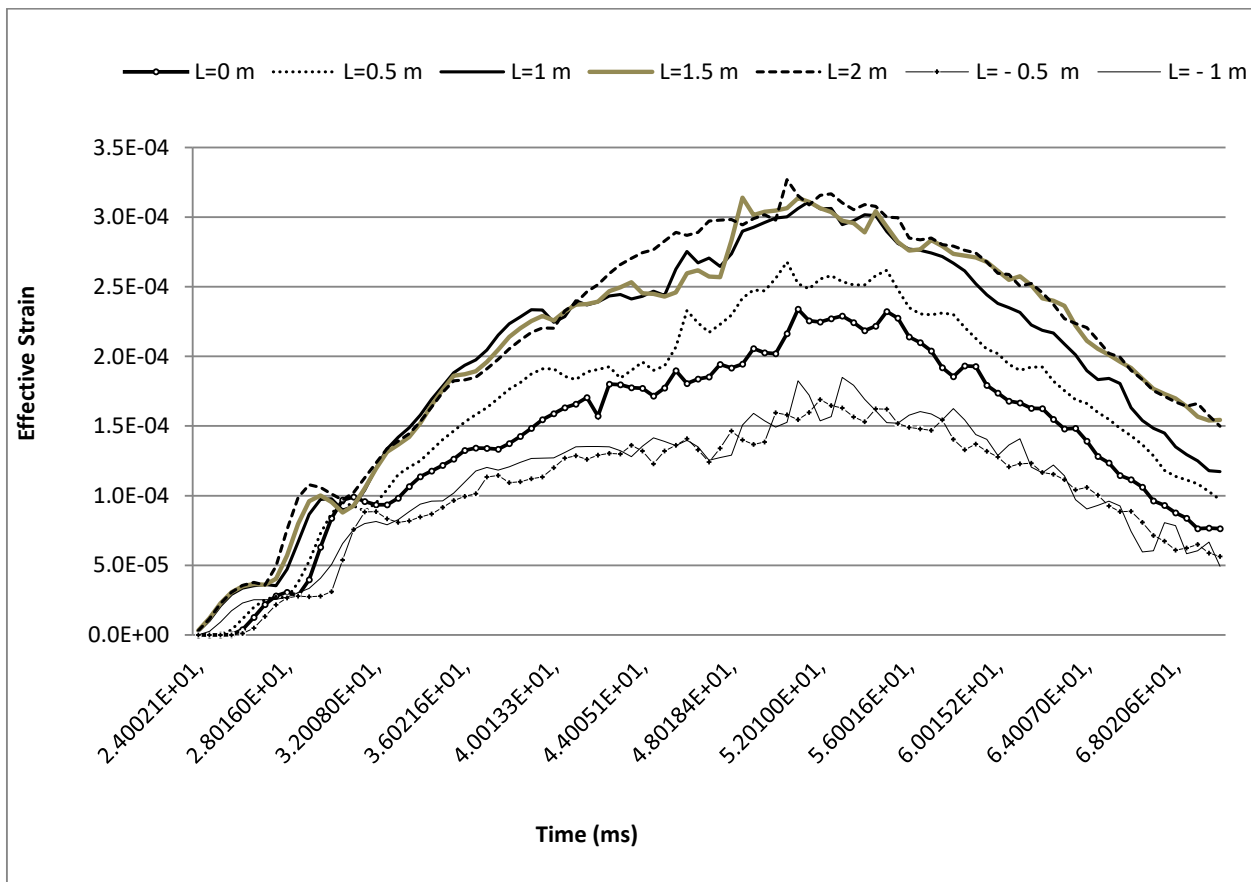


Fig. 12. Results for shifting the center of the second cavity, with the constant location of the first cavity (L).

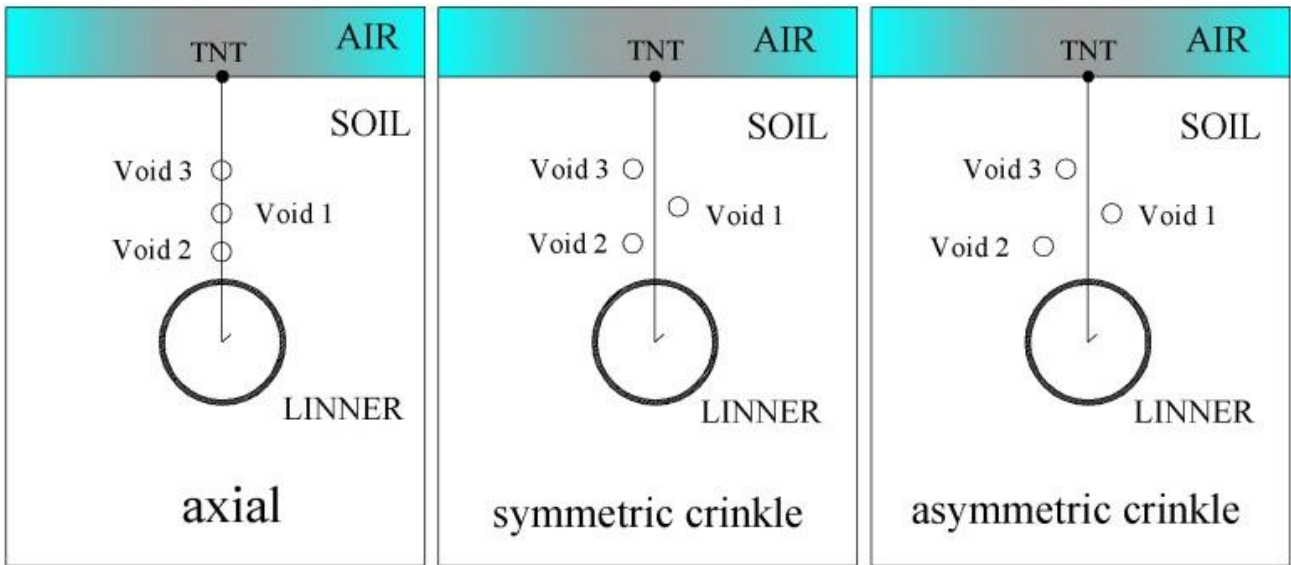


Fig. 13. Schematic of the model geometry used for assessing the effect of the axial direction and crinkles for cavities.

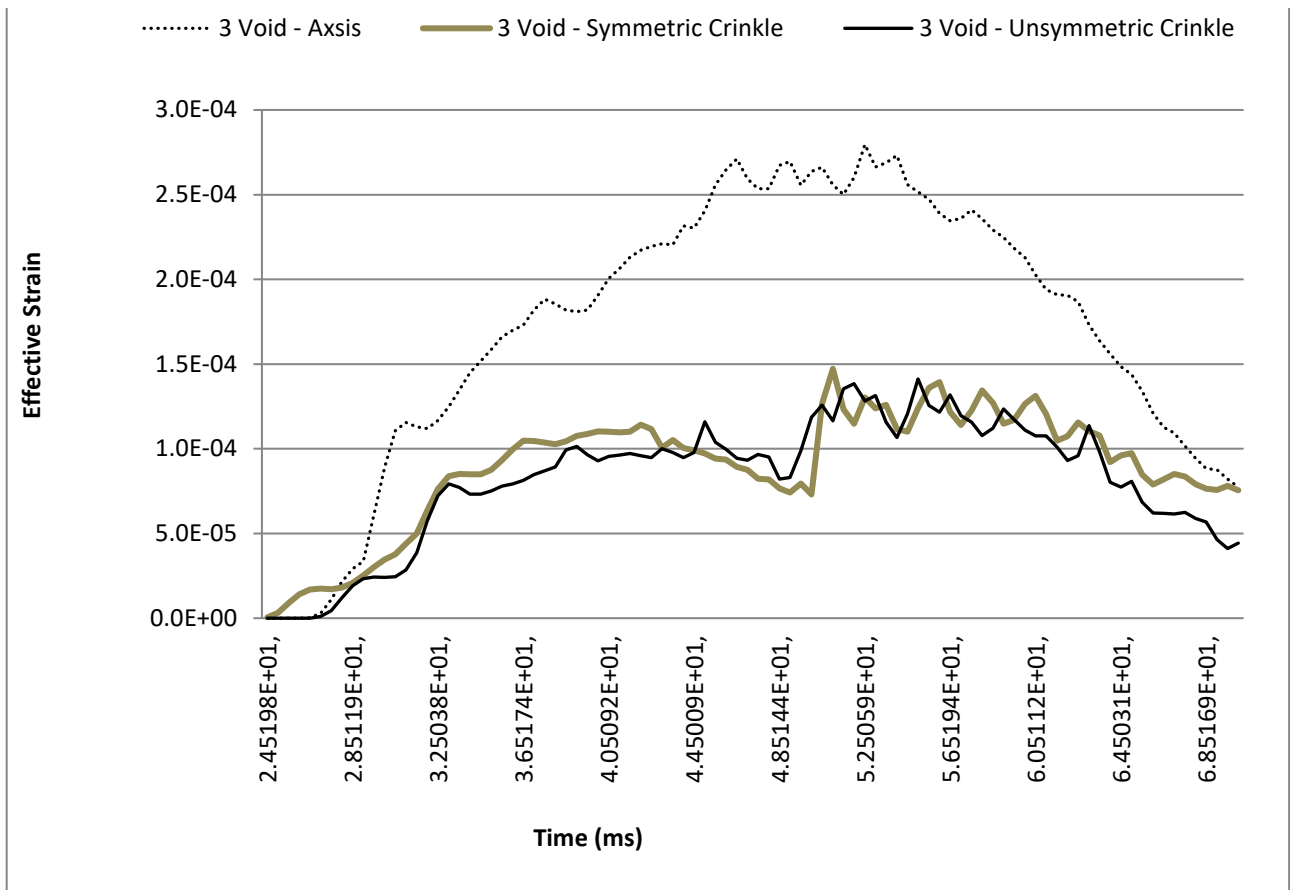


Fig. 14. Result for three different modes: axial, symmetric crinkle, and asymmetric crinkle.

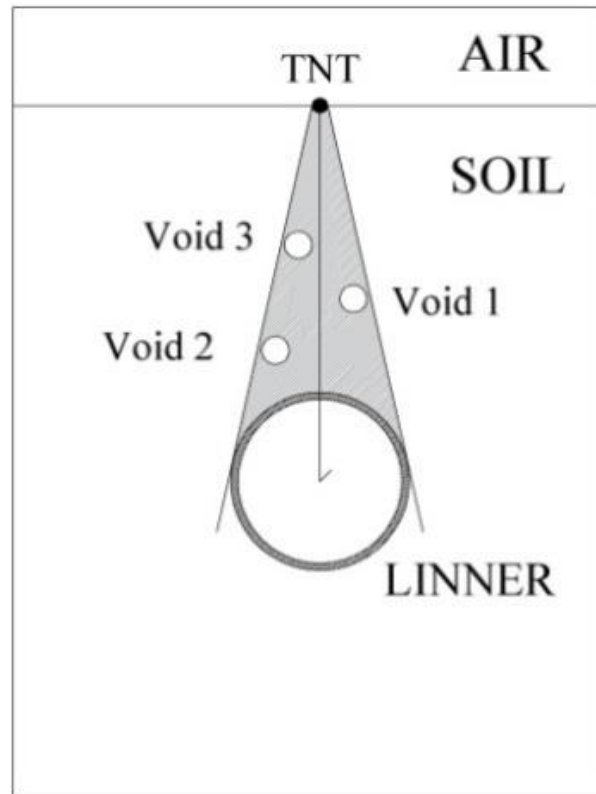


Fig. 15. The optimum range for positioning of the tunnel protective cavities.

References

- [1] Y. Lu, Z. Wang, K. Chong, A comparative study of buried structure in soil subjected to blast load using 2D and 3D numerical simulations, *Soil Dynamics and Earthquake Engineering*, 25(4) (2005) 275-288.
- [2] Z. Wang, Y. Lu, H. Hao, K. Chong, A full coupled numerical analysis approach for buried structures subjected to subsurface blast, *Computers & Structures*, 83(4) (2005) 339-356.
- [3] B. Luccioni, D. Ambrosini, S.C.K. Yuen, G. Nurick, Effects of Large and Spread Explosives Loads, *International Journal of Protective Structures*, 1(3) (2010) 319-344.
- [4] N. Nagy, M. Mohamed, J.C. Boot, Mtc, Egypt, Nonlinear numerical modeling for the effects of surface explosions on buried reinforced concrete structures, *Geomechanics and Engineering*, 2 (2010) 1-18.
- [5] H.L. Chen, Z.C. Xia, J.N. Zhou, H.L. Fan, F.N. Jin, Dynamic responses of underground arch structures subjected to conventional blast loads: Curvature effects, *Archives of Civil and Mechanical Engineering*, 13(3) (2013) 322-333.
- [6] X.F. Deng, J.B. Zhu, S.G. Chen, Z.Y. Zhao, Y.X. Zhou, J. Zhao, Numerical study on tunnel damage subject to blast-induced shock wave in jointed rock masses, *Tunnelling and Underground Space Technology*, 43 (2014) 88-100.
- [7] B. Mobaraki, M. Vaghefi, Numerical study of the depth and cross-sectional shape of tunnel under surface explosion, *Tunnelling and Underground Space Technology*, 47 (2015) 114-122.
- [8] L. Laine, A. Sandvik, Derivation of mechanical properties for sand, in: *Proceedings of the 4th Asia-Pacific Conference on Shock and impact loads on structures*, CI-Premier PTE LTD, Singapore, ANSYS Inc., 2001, pp. 368.
- [9] B. Pandurangan, Development, parameterization and validation of dynamic material models for soil and transparent armor glass, *Clemson University*, 2009.
- [10] U.S.D.o.t.A. TM5-855-1., *Fundamentals of protective design for conventional weapons*, Headquarters, Dept. of the Army, [Washington, DC], 1986.
- [11] P. Vannucci, F. Masi, I. Stefanou, A study on the simulation of blast actions on a monument structure, (2017).
- [12] E. Lee, M. Finger, W. Collins, *JWL equation of state coefficients for high explosives*, UCID-16189 United States 10.2172/4479737 Dep. NTIS LLNL English, Lawrence Livermore National Lab. (LLNL), Livermore, CA (United States), 1973.
- [13] M.A. Yusof, R.N. Rosdi, N.M. Nor, A. Ismail, M.A. Yahya, N.C. Peng, Simulation of reinforced concrete blast wall subjected to air blast loading, *Journal of Asian scientific research*, 4(9) (2014) 522-533.

- [14] B. Zakrisson, Numerical and experimental studies of blast loading, Luleå tekniska universitet, 2010.
- [15] P. Zhang, Y. Cheng, J. Liu, Numerical analysis of dynamic response of corrugated core sandwich panels subjected to near-field air blast loading, *Shock and Vibration*, 2014 (2014).
- [16] G.F.C. Rogers, Y.R. Mayhew, Thermodynamic and transport properties of fluids: SI units, Blackwell, Oxford, 2003.
- [17] Y.D. Murray, Users manual for LS-DYNA concrete material model 159, 2007.
- [18] Y. Lu, Z. Wang, Characterization of structural effects from above-ground explosion using coupled numerical simulation, *Computers & Structures*, 84(28) (2006) 1729-1742.
- [19] R.M. Brannon, S. Leelavanichkul, Survey of four damage models for concrete, Sandia National Laboratories, 32(1) (2009) 1-80.
- [20] Ansys Inc, Autodyn theory manual revision 4.3, in, 2005.
- [21] J. Leppänen, Concrete structures subjected to fragment impacts, Chalmers University of Technology, 2004.
- [22] A.J. Castellano, J.P. Caltagirone, F.E. Sock, N. Dobbs, A.A. RESEARCH, D.C.S.L. MO., Structures to Resist the Effects of Accidental Explosions (TM 5-1300, NAVFAC P-397, AFM 88-22). Revision of Tri-Service Regulatory Design Manual, Defense Technical Information Center, 1982.

HOW TO CITE THIS ARTICLE

H. Hosseini-Nassab, S.M. Movahedifar, Evaluation of Protective Cavities Position on Decreasing Destructive Effects of Surface Blast on Buried Tunnels, *AUT J. Civil Eng.*, 4(4) (2020) 543-556

DOI: [10.22060/ajce.2020.17101.5614](https://doi.org/10.22060/ajce.2020.17101.5614)

